Metric-signature topological transitions in dispersive metamaterials

E. Reyes-Gómez,[1] S. B. Cavalcanti,[2] L. E. Oliveira,[3] and C. A. A. de Carvalho[4]

[1]*Instituto de Física, Facultad de Ciencias Exactas y Naturales, Universidad de Antioquia UdeA, Calle 70 No. 52-21, Medellín, Colombia*
[2]*Instituto de Física, Universidade Federal de Alagoas, Maceió, Alagoas 57072-970, Brazil*
[3]*Instituto de Física, Universidade Estadual de Campinas - Unicamp, Campinas, São Paulo 13083-859, Brazil*
[4]*CNPEM, Caixa Postal 6192, Campinas, São Paulo 13083-970, Brazil*

The metric signature topological transitions associated with the propagation of electromagnetic waves in a dispersive metamaterial with frequency-dependent and anisotropic dielectric and magnetic responses are examined in the present work. The components of the reciprocal-space metric tensor depend upon both the electric permittivity and magnetic permeability of the metamaterial, which are taken as Drude-like dispersive models. A thorough study of the frequency dependence of the metric tensor is presented which leads to the possibility of topological transitions of the isofrequency surface determining the wave dynamics inside the medium, to a diverging photonic density of states at some range of frequencies, and to the existence of large wave vectors' modes propagating through the metamaterial.

PACS number(s): 41.20.−q, 78.20.Ci, 42.50.Ct, 78.67.Pt

I. INTRODUCTION

Condensed matter systems may provide laboratory realizations of cosmological scenarios thanks to analogous mathematical descriptions that ultimately allow us to relate physical properties in those distinct settings [1]. Analogies in the mathematical descriptions of different physical systems have often been used as a tool to further our understanding. A celebrated example is that of photonic crystals [2,3], where much has been learned about photon dynamics by drawing on the similarities with electron dynamics in crystalline solids. In the case of photonic crystals, Maxwell's equations in periodically arranged media of different electric permittivities (ϵ) and magnetic permeabilities (μ) are similar in form to Schrödinger's equation for electrons propagating in the periodic potential of a crystalline solid.

A more recent example [4] draws upon the analogous form of Maxwell's equations in curved space-time and in a related material medium. The electric and magnetic responses of the medium are obtained from the gravitational metric of the curved space-time, thus opening the possibility of testing a host of phenomena described by general relativity in laboratory experiments. All that is required is a reinterpretation of the equation for electromagnetism in curved space

$$\frac{1}{\sqrt{-g}}\,\partial_\beta(\sqrt{-g}\,F^{\alpha\beta}) = \frac{4\pi}{c}\,j^\alpha, \qquad (1)$$

as

$$\partial_\beta G^{\alpha\beta} = \frac{4\pi}{c}J^\alpha, \qquad (2)$$

upon identifying $G^{\alpha\beta} = \sqrt{-g}\,F^{\alpha\beta}$ and $J^\alpha = \sqrt{-g}\,j^\alpha$. Equation (2) can then be viewed as the equation for electromagnetism in a medium in flat space, if we define $D_i = G^{0i}$ and $H_i = \frac{1}{2}\epsilon_{ijk}G^{jk}$. We can then relate these quantities to $E_i = F_{i0}$ and $B_i = \frac{1}{2}\epsilon_{ijk}F_{jk}$. The constitutive relations are easily derived from the relation $G^{\alpha\beta} = \sqrt{-g}\,g^{\alpha\mu}g^{\beta\nu}F_{\mu\nu}$. Note that the metric intervenes as $(\vec{\mathbf{E}},\vec{\mathbf{B}})$ are defined in terms of a covariant tensor $F_{\alpha\beta}$, whereas $(\vec{\mathbf{D}},\vec{\mathbf{H}})$ are defined in terms of

a contravariant tensor $G^{\alpha\beta}$. Thus, the metric determines the electromagnetic responses in the flat space reinterpretation.

This correspondence has inspired the design of a number of experimental settings to test the transitions associated to metric signature changes in momentum space [5] and topological transitions [6], the relationship between statistical and cosmological time flow via the optical analog of a big-bang-like event [7], Hawking radiation [8], cosmological inflation [9], and the behavior of the vacuum in a strong magnetic field [10].

In the present work, we concentrate on the study of the transitions caused by signature changes in metrics in reciprocal space. We perform a systematic analysis of the cases that arise as we use various materials to induce such changes. We begin with anisotropic media that experience different signs for their electric permittivities, and go beyond by including dispersive metamaterials in our analysis. It is important to point out that, in practice, an isotropic left-handed material (LHM) is still a great challenge for researchers, as the available LHM structures are intrinsically anisotropic. A study of a semiconductor metamaterial with anisotropic dielectric response may be found in the work by Hoffman *et al.* [11], whereas for general anisotropic metamaterials, we refer to the studies by Krishnamoorthy *et al.* [6], Soukoulis *et al.* [12], Wilson [13], and Zheludev [14].

Artificial metamaterials [14–16] are also known as LHMs, due to their peculiar feature that light phase velocity travels in such materials in the opposite direction of the group velocity. Metamaterial structures are designed to achieve unusual electromagnetic properties, such as negative refraction, superlenses, optical magnetism, and cloaking, among others. Periodic, quasiperiodic, fractal, and disordered arrangements of layered one-dimensional positive-index material or metamaterial stacks have been extensively studied, and also exhibited unusual features, such as non-Bragg gaps, corresponding to zero average refractive index, plasmon-polariton gaps, and Anderson delocalization properties [17–24].

The use of artificially nanostructured metamaterials to mimic gravitational environments will certainly add new experimental situations to the ones already proposed in the

literature, which have not included those materials where both the electric and magnetic responses may be negative, thus leading to negative refraction indices. However, we have restricted our discussion to studying the behavior of electromagnetic fields that experience changes in the signature of the metric in reciprocal space associated to their dispersion relations, and the unusual phenomena that this brings about, such as the copious production of particles, dubbed "big flashes," that could also occur in Bose-Einstein condensates or in gravitational systems.

As real metamaterials are intrinsically dispersive materials, the present study analyzes the influence of dispersive electric and magnetic responses on the metric signature change phenomenon. The metric changes correspond to looking at different frequency ranges for light propagating in the metamaterials. The work is organized as follows. Section II presents the theoretical framework and numerical results concerning nonmagnetic materials with dielectric anisotropy, whereas Sec. III is devoted to the study of metric signature topological transitions in dielectric and magnetic anisotropic materials. Our conclusions are in Sec. IV.

II. NONMAGNETIC MATERIALS WITH DIELECTRIC ANISOTROPY

In the absence of free charges and electric currents, the Maxwell equations describing the behavior of the electromagnetic field in a continuous medium may be written as

$$\vec{\mathbf{k}} \times \vec{\mathbf{k}} \times \vec{\mathbf{E}}(\vec{\mathbf{k}},\omega) = \frac{\omega}{c} \vec{\mathbf{k}} \times [\overset{\leftrightarrow}{\boldsymbol{\mu}} \cdot \vec{\mathbf{H}}(\vec{\mathbf{k}},\omega)] \tag{3}$$

and

$$\vec{\mathbf{k}} \times \vec{\mathbf{k}} \times \vec{\mathbf{H}}(\vec{\mathbf{k}},\omega) = -\frac{\omega}{c} \vec{\mathbf{k}} \times [\overset{\leftrightarrow}{\boldsymbol{\epsilon}} \cdot \vec{\mathbf{E}}(\vec{\mathbf{k}},\omega)], \tag{4}$$

where $\overset{\leftrightarrow}{\boldsymbol{\mu}} = \overset{\leftrightarrow}{\boldsymbol{\mu}}(\vec{\mathbf{k}},\omega)$ and $\overset{\leftrightarrow}{\boldsymbol{\epsilon}} = \overset{\leftrightarrow}{\boldsymbol{\epsilon}}(\vec{\mathbf{k}},\omega)$ are the magnetic permeability and electric permittivity tensors, respectively, associated with the material medium.

Equations (3) and (4) may be used to study the metric signature transition in a wide variety of optical materials. Here, we first consider the case of nonmagnetic materials with dielectric anisotropy. In this case $\boldsymbol{\mu} = \overset{\leftrightarrow}{\mathbf{I}}$ and Eqs. (3) and (4) lead to

$$[\vec{\mathbf{k}} \cdot \vec{\mathbf{E}}(\vec{\mathbf{k}},\omega)]\vec{\mathbf{k}} - k^2 \vec{\mathbf{E}}(\vec{\mathbf{k}},\omega) = -\frac{\omega^2}{c^2} \overset{\leftrightarrow}{\boldsymbol{\epsilon}} \cdot \vec{\mathbf{E}}(\vec{\mathbf{k}},\omega). \tag{5}$$

Without loss of generality, one may assume that the tensor $\overset{\leftrightarrow}{\boldsymbol{\epsilon}}$ is diagonal. Otherwise, one may always perform a coordinate transformation to reduce $\overset{\leftrightarrow}{\boldsymbol{\epsilon}}$ to its diagonal form. Therefore,

$$\overset{\leftrightarrow}{\boldsymbol{\epsilon}} = (\epsilon_{ij}) = (\epsilon_j \delta_{ij}) \tag{6}$$

and

$$\left[k_l k_l \, \delta_{ij} - k_i k_l \, \delta_{lj} - \frac{\omega^2}{c^2} \epsilon_{ij} \right] E_j(\vec{\mathbf{k}},\omega) = 0. \tag{7}$$

The condition for solving the above system is

$$\det \left\| k_l k_l \, \delta_{ij} - k_i k_l \, \delta_{lj} - \frac{\omega^2}{c^2} \epsilon_{ij} \right\| = 0, \tag{8}$$

which determines the dispersion $\omega = \omega(\vec{\mathbf{k}})$. One may write Eq. (8) as

$$\epsilon_1 \epsilon_2 \epsilon_3 \frac{\omega^2}{c^2} \left[\frac{\omega^4}{c^4} - \frac{\omega^2}{c^2} \left(\frac{k_1^2 + k_2^2}{\epsilon_3} + \frac{k_1^2 + k_3^2}{\epsilon_2} + \frac{k_2^2 + k_3^2}{\epsilon_1} \right) \right.$$
$$\left. + \left(\frac{k_1^2}{\epsilon_2 \epsilon_3} + \frac{k_2^2}{\epsilon_1 \epsilon_3} + \frac{k_3^2}{\epsilon_1 \epsilon_2} \right) k^2 \right] = 0, \tag{9}$$

where $k^2 = k_1^2 + k_2^2 + k_3^2$. Here we focus our attention in uniaxial dielectric materials. In this case, $\epsilon_1 = \epsilon_2 = \epsilon_\perp$ and $\epsilon_3 = \epsilon_\parallel$, and Eq. (9) transforms into

$$\epsilon_\perp^2 \epsilon_\parallel \frac{\omega^2}{c^2} \left[\frac{k^2}{\epsilon_\perp} - \frac{\omega^2}{c^2} \right] \left[\frac{k_1^2}{\epsilon_\parallel} + \frac{k_2^2}{\epsilon_\parallel} + \frac{k_3^2}{\epsilon_\perp} - \frac{\omega^2}{c^2} \right] = 0, \tag{10}$$

which leads to the dispersion

$$\frac{k^2}{\epsilon_\perp} = \frac{\omega^2}{c^2} \tag{11}$$

corresponding to the ordinary ray, and to the dispersion relation

$$\frac{k_1^2}{\epsilon_\parallel} + \frac{k_2^2}{\epsilon_\parallel} + \frac{k_3^2}{\epsilon_\perp} = \frac{\omega^2}{c^2} \tag{12}$$

corresponding to the extraordinary ray. For isotropic materials one has $\epsilon_\perp = \epsilon_\parallel$, and Eq. (12) reduces to Eq. (11).

First we analyze the case of the extraordinary ray and suppose that both $\epsilon_\perp$ and $\epsilon_\parallel$ are functions of the frequency ω. By introducing the temporal component k_0 of the four-momentum k_μ as $k_0 = \omega/c$, Eq. (12) may be rewritten as

$$\frac{q_1^2}{\epsilon_\parallel} + \frac{q_2^2}{\epsilon_\parallel} + \frac{q_3^2}{\epsilon_\perp} = 1, \tag{13}$$

where $q_i = k_i/k_0$ $(i = 1, 2, 3)$ are the three dimensionless spatial components of the four-momentum k_μ. The above equation allows to obtain the isofrequency surface in the $\vec{\mathbf{k}}$ space at a given frequency ω.

Let us now turn to Fig. 1, where we have depicted the isofrequency surfaces for various metrics, assuming a Drude-like electric response, i.e,

$$\epsilon_\alpha(\omega) = \epsilon_\alpha^0 \left(1 - \frac{\omega_{e\alpha}^2}{\omega^2} \right), \tag{14}$$

with $\alpha = \perp, \parallel$. Figures 1(a), 1(b), and 1(d) where obtained for $\epsilon_\perp^0 = 1.21, \epsilon_\parallel^0 = 1, \omega_{e\perp} = 2\pi$ GHz, and $\omega_{e\parallel} = 6\pi$ GHz, at the frequencies $\nu = \omega/(2\pi) = 3.5$ GHz, $\nu = 2$ GHz, and $\nu = 0.5$ GHz, respectively. Notice that $\epsilon_\alpha < 0$ ($\epsilon_\alpha > 0$) if $\nu < \nu_{e\alpha}$ ($\nu > \nu_{e\alpha}$), with $\nu_{e\alpha} = \omega_{e\alpha}/(2\pi)$ and $\alpha = \perp, \parallel$. Here $\nu_{e\perp} = 1$ GHz and $\nu_{e\parallel} = 3$ GHz are the transversal and longitudinal plasmon frequencies, respectively, determining the frequency ranges where $\epsilon_\perp$ and $\epsilon_\parallel$ are positive or negative. The results depicted in Fig. 1(c) were obtained, at $\nu = 2.5$ GHz, for the same values of $\epsilon_\perp^0, \epsilon_\parallel^0$, but by taking $\omega_{e\perp} = 6\pi$ GHz, and $\omega_{e\parallel} = 2\pi$ GHz. In this case the transversal and longitudinal plasmon frequencies determining the sign of $\epsilon_\perp$ and $\epsilon_\parallel$, respectively, are $\nu_{e\perp} = 3$ GHz and $\nu_{e\parallel} = 1$ GHz, respectively.

If for a given value of the frequency ω one has $\epsilon_\perp > 0$ and $\epsilon_\parallel > 0$, the isofrequency surface defined in the real $\vec{\mathbf{k}}$ space by the equation $\omega(\vec{\mathbf{k}}) = $ const is an ellipsoid, as one may see from Fig. 1(a). If $\epsilon_\perp > 0$ and $\epsilon_\parallel < 0$, then the isofrequency surface
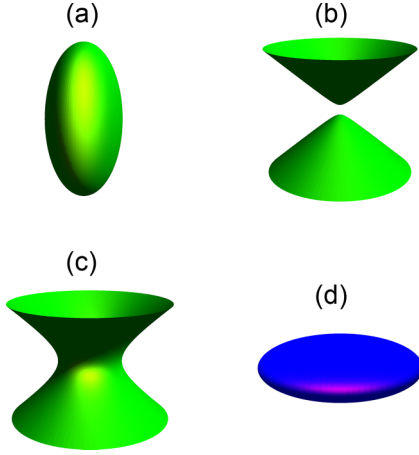
FIG. 1. (Color online) Isofrequency surfaces, corresponding to the extraordinary ray, for different metrics in the flat Minkowski space-time. Panels (a), (b), and (d) were obtained for $\epsilon_\perp^0 = 1.21$, $\epsilon_\parallel^0 = 1$, $\omega_{e\perp} = 2\pi$ GHz, and $\omega_{e\parallel} = 6\pi$ GHz [cf. Eq. (14)], at the frequencies $\nu = \omega/(2\pi) = 3.5$ GHz, $\nu = 2$ GHz, and $\nu = 0.5$ GHz, respectively. These cases correspond to metrics $(-,+,+,+)$, $(-,-,-,+)$, and $(-,-,-,-)$, respectively. In panel (c) we chose $\nu = 2.5$ GHz and the same values of $\epsilon_\perp^0, \epsilon_\parallel^0$, but $\omega_{e\perp} = 6\pi$ GHz, and $\omega_{e\parallel} = 2\pi$ GHz. The corresponding metric is $(-,+,+,-)$ in this case.
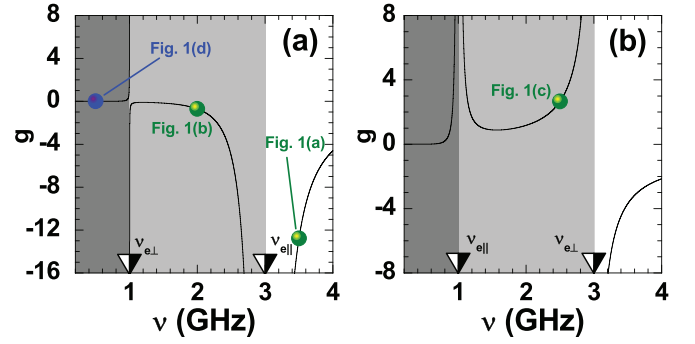

FIG. 2. (Color online) Determinant g of the metric tensor $(g_{\mu\nu})$ as a function of the frequency. Panel (a) was obtained for the set of parameters $\epsilon_\perp^0 = 1.21$, $\epsilon_\parallel^0 = 1$, $\omega_{e\perp} = 2\pi$ GHz, and $\omega_{e\parallel} = 6\pi$ GHz, whereas in panel (b) we used the same values of $\epsilon_\perp^0$ and $\epsilon_\parallel^0$, but we took $\omega_{e\perp} = 6\pi$ GHz and $\omega_{e\parallel} = 2\pi$ GHz. Dark-gray and white areas in panels (a) and (b) represent the frequency regions with metrics $(-,-,-,-)$ and $(-,+,+,+)$, respectively, whereas the intermediate gray area in Fig. 2(a) [Fig. 2(b)] represents a bandwidth with a metric $(-,-,-,+)$ [$(-,+,+,-)$]. Triangles at the horizontal axis are located at the transition (plasmon) frequencies between different metrics. The frequency values corresponding to full dots depicted in both panels were used to compute the results of Fig. 1.

defined in the real $\vec{k}$ space is a two-sheeted hyperboloid, whereas if $\epsilon_\perp < 0$ and $\epsilon_\parallel > 0$ such surface is a one-sheeted hyperboloid [cf. Figs. 1(b) and 1(c), respectively]. Finally, if $\epsilon_\perp < 0$ and $\epsilon_\parallel < 0$ at certain values of ω, the isofrequency surface does not admit any representation in the real $\vec{k}$ space, but is an ellipsoid in the imaginary $i\vec{k}$ space [cf. Fig. 1(d)]. The dispersion relation for the extraordinary ray is not obtained in this case.

By introducing the metric four-tensor with components $g_{\mu\nu}$, Eq. (12) for the extraordinary ray may be rewritten as

$$g_{\mu\nu}\, k_\mu k_\nu = 0, \tag{15}$$

where

$$(g_{\mu\nu}) = \begin{pmatrix} -1 & 0 & 0 & 0 \\ 0 & \epsilon_\parallel^{-1} & 0 & 0 \\ 0 & 0 & \epsilon_\parallel^{-1} & 0 \\ 0 & 0 & 0 & \epsilon_\perp^{-1} \end{pmatrix}. \tag{16}$$

The metric tensor $(g_{\mu\nu})$ defines the metric of the $\vec{k}$ space determining the dispersion relation for the extraordinary ray in the anisotropic nonmagnetic dielectric medium. As the metric tensor is diagonal in this case, such a metric may be denoted as $[-1, \mathrm{sign}(g_{11}), \mathrm{sign}(g_{22}), \mathrm{sign}(g_{33})]$. The frequency dependence of both $\epsilon_\parallel$ and $\epsilon_\perp$ leads to the existence of different frequency regions of the spectrum with different metric signatures. For instance, if $\epsilon_\perp > 0$ and $\epsilon_\parallel > 0$ for a given value of ω, then we have the metric $(-,+,+,+)$ of the ordinary flat Minkowski space [cf. Fig. 1(a)]. If $\epsilon_\perp > 0$ and $\epsilon_\parallel < 0$ then we have the three-time metric $(-,-,-,+)$, whereas if $\epsilon_\perp < 0$ and $\epsilon_\parallel > 0$ then the two-time metric $(-,+,+,-)$ is achieved [cf. Figs. 1(b) and 1(c), respectively]. If $\epsilon_\perp < 0$ and $\epsilon_\parallel < 0$ then we have the four-time metric $(-,-,-,-)$ [cf. Fig. 1(d)]. As

mentioned, no dispersion relation for the extraordinary ray is obtained in this case, so the four-time metric is not feasible.

In addition,

$$g = \det \|g_{\mu\nu}\| = -\frac{1}{\epsilon_\parallel^2 \, \epsilon_\perp} \tag{17}$$

is also a function of the frequency which may change depending on the metric of the $\vec{k}$ space determining the dispersion relation. In this sense, one may note that $g < 0$ for the metrics $(-,+,+,+)$ and $(-,-,-,+)$, whereas $g > 0$ for the metrics $(-,+,+,-)$ and $(-,-,-,-)$. We display in Fig. 2 the determinant g of the metric tensor $(g_{\mu\nu})$ as a function of the frequency. The results displayed in Fig. 2(a) were obtained for $\epsilon_\perp^0 = 1.21$, $\epsilon_\parallel^0 = 1$, $\omega_{e\perp} = 2\pi$ GHz, and $\omega_{e\parallel} = 6\pi$ GHz, whereas the results depicted in Fig. 2(b) were computed for the same values of $\epsilon_\perp^0$ and $\epsilon_\parallel^0$, but for $\omega_{e\perp} = 6\pi$ GHz and $\omega_{e\parallel} = 2\pi$ GHz. The dark-gray and white areas in both Figs. 2(a) and 2(b) correspond to metrics $(-,-,-,-)$ and $(-,+,+,+)$, respectively, whereas the intermediate gray area in Fig. 2(a) [Fig. 2(b)] corresponds to a metric $(-,-,-,+)$ [$(-,+,+,-)$]. The triangles at the bottom axes of both Figs. 2(a) and 2(b) are located at the plasmon frequencies, i.e., at the transition frequencies between different metrics. The frequency values [$\nu = \omega/(2\pi)$] corresponding to full dots depicted in Fig. 2 were used to compute the results displayed in Fig. 1.

To explore the role played by the different metrics in the structure of the dispersion relation, we have displayed in Fig. 3 the dispersion $\nu = \nu(\vec{k})$. The dashed and solid lines correspond to solutions for the ordinary [cf. Eq. (11)] and extraordinary rays [Eq. (12)], respectively, in the case of uniaxial nonmagnetic anisotropic materials with the anisotropy axis along the z direction. The calculations shown in Figs. 3(a) and 3(b) were
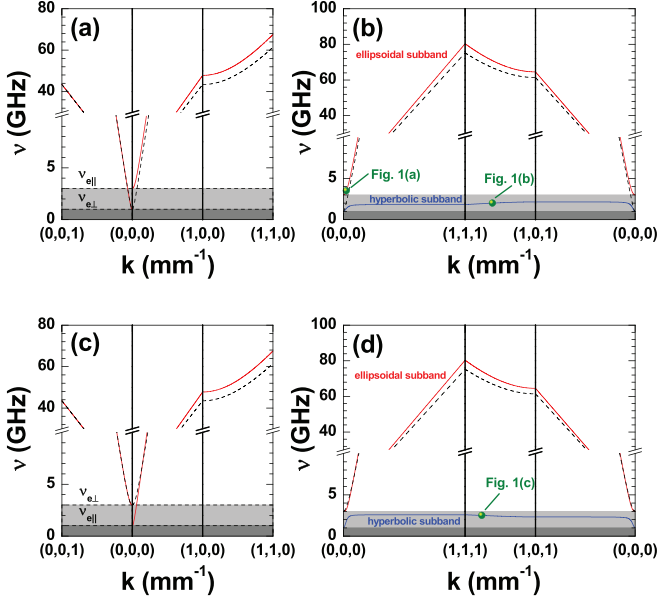
FIG. 3. (Color online) Dispersion relation $\nu = \nu(\vec{k})$ [$\nu = \omega/(2\pi)$] obtained from Eq. (11) for the ordinary ray (dashed lines) and from Eq. (12) for the extraordinary ray (solid lines) in the case of uniaxial nonmagnetic anisotropic materials. Results depicted in panels (a) and (b) were obtained for the set of parameters $\epsilon_\perp^0 = 1.21$, $\epsilon_\parallel^0 = 1$, $\omega_{e\perp} = 2\pi$ GHz, and $\omega_{e\parallel} = 6\pi$ GHz, whereas in panels (c) and (d) we used the same values of $\epsilon_\perp^0$ and $\epsilon_\parallel^0$, but we took $\omega_{e\perp} = 6\pi$ GHz and $\omega_{e\parallel} = 2\pi$ GHz. Dark-gray and white areas in all panels represent the frequency regions with the forbidden $(-,-,-,-)$ and normal $(-,+,+,+)$ metrics, respectively. The intermediate gray area in both panels (a) and (b) corresponds to the bandwidth with metric $(-,-,-,+)$, whereas in panels (c) and (d) such intermediate gray regions correspond to the two-time metric $(-,+,+,-)$. Horizontal dashed lines in panels (a) and (c) correspond to the plasmon-frequency values at which transitions between different metrics take place. The frequency values corresponding to full dots depicted in panels (b) and (d) were used to obtain the corresponding results of Fig. 1.

obtained by setting $\epsilon_\perp^0 = 1.21$, $\epsilon_\parallel^0 = 1$, $\omega_{e\perp} = 2\pi$ GHz, and $\omega_{e\parallel} = 6\pi$ GHz in Eq. (14). The results depicted in Figs. 3(c) and 3(d) were obtained by using the same values of $\epsilon_\perp^0$ and $\epsilon_\parallel^0$, but by taking $\omega_{e\perp} = 6\pi$ GHz and $\omega_{e\parallel} = 2\pi$ GHz. In all panels of Fig. 3, the dark-gray and white areas represent the frequency regions with the forbidden $(-,-,-,-)$ and normal $(-,+,+,+)$ metrics, respectively. The intermediate gray areas in both Figs. 3(a) and 3(b) correspond to the bandwidth with the three-time metric $(-,-,-,+)$, whereas in Figs. 3(c) and 3(d) such regions correspond to the two-time metric $(-,+,+,-)$. The plasmon-frequency values at which transitions between different metrics take place are represented by horizontal dashed lines in both Figs. 3(a) and 3(c). The frequency values corresponding to full dots shown in both Figs. 3(b) and 3(d) were used to compute the corresponding results of Fig. 1.

As we have chosen $\epsilon_1 = \epsilon_2 = \epsilon_\perp$ and $\epsilon_3 = \epsilon_\parallel$ in Eq. (6), the present model describes a uniaxial dielectric with the anisotropy axis along the z direction. If the wave vector $\vec{k}$ is perpendicular to the z axis then the vector field $\vec{D}$ may be

decomposed into a component parallel and other perpendicular to the anisotropy axis, which are also perpendicular to $\vec{k}$. In this case Maxwell's equations admit two uncoupled solutions with orthogonal polarizations. The component of $\vec{D}$ oscillating along the z axis leads to the extraordinary ray, whereas the perpendicular component originates the ordinary ray. On the other hand, if the wave vector $\vec{k}$ is parallel to the anisotropy axis then the vector field $\vec{D}$ only oscillates in a plane perpendicular to z. As all the spatial directions over such a plane are equivalent, Maxwell's equations then admit two degenerated solutions corresponding to the ordinary ray, i.e., the extraordinary-ray solution in fact reduces to the ordinary-ray solution in this case. This physical situation may be seen in both Figs. 3(a) and 3(c), where the wave vector $\vec{k}$ is continuously changed in the sequence $(0,0,1) \to (0,0,0) \to (1,0,0) \to (1,1,0)$. One may note from Figs. 3(a) and 3(c) that, when the wave vector $\vec{k}$ is perpendicular to the z axis, one obtains a solution corresponding to the extraordinary ray that is not observed when the wave vector $\vec{k}$ is parallel to the anisotropy axis. The continuity of this particular mode at the $\vec{k} = 0$ (Γ) point is not achieved. Nevertheless, the electromagnetic mode corresponding to the ordinary ray exhibits a continuous behavior at the Γ point, as expected [see the dashed lines in both Figs. 3(a) and 3(c)].

If the wave vector $\vec{k}$ is neither perpendicular nor parallel to the z axis, then it is not possible to separate the spatial components of $\vec{k}$ parallel and perpendicular to the anisotropy axis in Eq. (12). In this case, depending on the behavior of the dielectric tensor as a function of the frequency, it is possible to obtain more than one solution from Eq. (12) corresponding to the extraordinary ray. For the Drude-like dielectric response considered here [cf. Eq. (14)], we have obtained two different modes for the extraordinary ray, apart from the electromagnetic mode corresponding to the ordinary ray. Numerical results are displayed in Figs. 3(b) and 3(d), where the wave vector $\vec{k}$ varies according to the sequence $(0,0,0) \to (1,1,1) \to (1,0,1) \to (0,0,0)$ to guarantee the obliqueness of $\vec{k}$ with respect to the anisotropy axis. It is apparent from Figs. 3(b) and 3(d) that one of the extraordinary subbands lies in the region of the metric $(-,+,+,+)$, where the isofrequency surface is an ellipsoid [cf. Fig. 1(a)]. One then may refer to this subband as an ellipsoidal subband. Particularly, for the Drude-like dielectric response considered here, the hyperbolic dispersion occurs only for the three-time $(-,-,-,+)$ and two-time $(-,+,+,-)$ metrics [cf. Figs. 1(b) and 1(c), respectively]. Therefore, such kinds of dispersions may only be exhibited by the so-called hyperbolic subband labeled in both Figs. 3(b) and 3(d). One may note that the hyperbolic subbands are bounded by the two plasmon frequencies associated with $\epsilon_\parallel$ and $\epsilon_\perp$. In other words, the metric transitions occur at the $\omega_{e\parallel}$ and $\omega_{e\perp}$ plasmon frequencies [cf. Eq. (17) and Figs. 2 and 3].

III. DIELECTRIC AND MAGNETIC ANISOTROPIC MATERIALS

We now consider a material with both dielectric and magnetic anisotropy, and suppose that the electric permittivity and magnetic permeability tensors are both diagonal, with components ϵ_i and μ_i ($i = 1, 2, 3$), respectively. In this

case,

$$\vec{\mathbf{k}} \times \vec{\mathbf{E}}(\vec{\mathbf{k}},\omega) = \frac{\omega}{c}\, \overleftrightarrow{\boldsymbol{\mu}} \cdot \vec{\mathbf{H}}(\vec{\mathbf{k}},\omega), \tag{18a}$$

$$\vec{\mathbf{k}} \times \vec{\mathbf{H}}(\vec{\mathbf{k}},\omega) = -\frac{\omega}{c}\, \overleftrightarrow{\boldsymbol{\epsilon}} \cdot \vec{\mathbf{E}}(\vec{\mathbf{k}},\omega). \tag{18b}$$

The set of Eqs. (18) may be written in matrix form as

$$\begin{pmatrix} 0 & -k_3 & k_2 & -\frac{\omega}{c}\mu_1 & 0 & 0 \\ k_3 & 0 & -k_1 & 0 & -\frac{\omega}{c}\mu_2 & 0 \\ -k_2 & k_1 & 0 & 0 & 0 & -\frac{\omega}{c}\mu_3 \\ \frac{\omega}{c}\epsilon_1 & 0 & 0 & 0 & -k_3 & k_2 \\ 0 & \frac{\omega}{c}\epsilon_2 & 0 & k_3 & 0 & -k_1 \\ 0 & 0 & \frac{\omega}{c}\epsilon_3 & -k_2 & k_1 & 0 \end{pmatrix} \begin{pmatrix} E_1 \\ E_2 \\ E_3 \\ H_1 \\ H_2 \\ H_3 \end{pmatrix} = 0. \tag{19}$$

The condition to solve the above system is

$$\det \begin{Vmatrix} 0 & -k_3 & k_2 & -\frac{\omega}{c}\mu_1 & 0 & 0 \\ k_3 & 0 & -k_1 & 0 & -\frac{\omega}{c}\mu_2 & 0 \\ -k_2 & k_1 & 0 & 0 & 0 & -\frac{\omega}{c}\mu_3 \\ \frac{\omega}{c}\epsilon_1 & 0 & 0 & 0 & -k_3 & k_2 \\ 0 & \frac{\omega}{c}\epsilon_2 & 0 & k_3 & 0 & -k_1 \\ 0 & 0 & \frac{\omega}{c}\epsilon_3 & -k_2 & k_1 & 0 \end{Vmatrix} = 0, \tag{20}$$

which leads to

$$\epsilon_1\epsilon_2\epsilon_3\mu_1\mu_2\mu_3 \frac{\omega^2}{c^2} \left\{ \frac{\omega^4}{c^4} - \frac{\omega^2}{c^2}\left[\frac{1}{\epsilon_3}\left(\frac{k_1^2}{\mu_2} + \frac{k_2^2}{\mu_1} \right) \right. \right.$$
$$+ \frac{1}{\epsilon_2}\left(\frac{k_1^2}{\mu_3} + \frac{k_3^2}{\mu_1} \right) + \frac{1}{\epsilon_1}\left(\frac{k_2^2}{\mu_3} + \frac{k_3^2}{\mu_2} \right) \bigg]$$
$$\left. + \left(\frac{k_1^2}{\epsilon_2\epsilon_3} + \frac{k_2^2}{\epsilon_1\epsilon_3} + \frac{k_3^2}{\epsilon_1\epsilon_2} \right)\left(\frac{k_1^2}{\mu_2\mu_3} + \frac{k_2^2}{\mu_1\mu_3} + \frac{k_3^2}{\mu_1\mu_2} \right) \right\}$$
$$= 0. \tag{21}$$

If we take $\epsilon_1 = \epsilon_2 = \epsilon_\perp$, $\epsilon_3 = \epsilon_\parallel$, $\mu_1 = \mu_2 = \mu_\perp$, and $\mu_3 = \mu_\parallel$, then Eq. (21) becomes

$$\epsilon_\perp^2 \epsilon_\parallel \mu_\perp^2 \mu_\parallel \frac{\omega^2}{c^2} \left[\frac{1}{\mu_\perp}\left(\frac{k_1^2}{\epsilon_\parallel} + \frac{k_2^2}{\epsilon_\parallel} + \frac{k_3^2}{\epsilon_\perp} \right) - \frac{\omega^2}{c^2} \right]$$
$$\times \left[\frac{1}{\epsilon_\perp}\left(\frac{k_1^2}{\mu_\parallel} + \frac{k_2^2}{\mu_\parallel} + \frac{k_3^2}{\mu_\perp} \right) - \frac{\omega^2}{c^2} \right] = 0. \tag{22}$$

The two possible dispersion relations are

$$\frac{1}{\mu_\perp}\left(\frac{k_1^2}{\epsilon_\parallel} + \frac{k_2^2}{\epsilon_\parallel} + \frac{k_3^2}{\epsilon_\perp} \right) - \frac{\omega^2}{c^2} = 0 \tag{23}$$

and

$$\frac{1}{\epsilon_\perp}\left(\frac{k_1^2}{\mu_\parallel} + \frac{k_2^2}{\mu_\parallel} + \frac{k_3^2}{\mu_\perp} \right) - \frac{\omega^2}{c^2} = 0, \tag{24}$$

with the corresponding metric tensors

$$\left(g_{\mu\nu}^{(1)} \right) = \begin{pmatrix} -1 & 0 & 0 & 0 \\ 0 & (\mu_\perp \epsilon_\parallel)^{-1} & 0 & 0 \\ 0 & 0 & (\mu_\perp \epsilon_\parallel)^{-1} & 0 \\ 0 & 0 & 0 & (\mu_\perp \epsilon_\perp)^{-1} \end{pmatrix} \tag{25}$$

TABLE I. Parameters used for the Drude-like electric and magnetic responses.

α	ϵ_α^0	$\omega_{e\alpha}/(2\pi)$ (GHz)	μ_α^0	$\omega_{m\alpha}/(2\pi)$ (GHz)
$\perp$	1.21	1.00	1.00	2.00
$\parallel$	1.00	3.00	1.21	4.00

and

$$\left(g_{\mu\nu}^{(2)} \right) = \begin{pmatrix} -1 & 0 & 0 & 0 \\ 0 & (\epsilon_\perp \mu_\parallel)^{-1} & 0 & 0 \\ 0 & 0 & (\epsilon_\perp \mu_\parallel)^{-1} & 0 \\ 0 & 0 & 0 & (\epsilon_\perp \mu_\perp)^{-1} \end{pmatrix}, \tag{26}$$

respectively. The determinants of $(g_{\mu\nu}^{(1)})$ and $(g_{\mu\nu}^{(2)})$ are

$$g^{(1)} = -\frac{1}{\mu_\perp^3 \epsilon_\parallel^2 \epsilon_\perp} \tag{27}$$

and

$$g^{(2)} = -\frac{1}{\epsilon_\perp^3 \mu_\parallel^2 \mu_\perp}, \tag{28}$$

respectively.

Here we consider Drude-like electric and magnetic responses for the metamaterial, i.e.,

$$\epsilon_\alpha(\omega) = \epsilon_\alpha^0 \left(1 - \frac{\omega_{e\alpha}^2}{\omega^2} \right) \tag{29}$$

and

$$\mu_\alpha(\omega) = \mu_\alpha^0 \left(1 - \frac{\omega_{m\alpha}^2}{\omega^2} \right), \tag{30}$$

with $\alpha = \perp$, $\parallel$. Notice that the sign of both ϵ_α and μ_α change at their corresponding plasmon frequencies. Therefore, such plasmon frequencies determine the set of frequency subbands with different associated metrics. In what follows, the parameters used in the calculations are given in Table I. Figure 4 then displays the calculated values for $g^{(1)}$ and $g^{(2)}$ in the case of a material with both dielectric and magnetic anisotropy. Of course, the determinants $g^{(1)}$ and $g^{(2)}$ of the metric tensors are functions of the frequency and diverge [see Eqs. (27) and (28)] at the corresponding metric signature transitions, which occur at the $\nu_{e\alpha}$ and $\nu_{m\alpha}$ electric and magnetic plasmon frequencies. Notice that the white and gray areas in all panels of Fig. 4 correspond to the normal Minkowski metric $(-, +, +, +)$ and three-time metric $(-, -, -, +)$, respectively, whereas the dark-gray area in Fig. 4(a) [Fig. 4(b)] corresponds to the metric $(-, +, +, -)$ $[(-, -, -, -)]$.

We have obtained the $\nu = \nu(\vec{\mathbf{k}})$ dispersion and results are given in Figs. 5 and 6, with the calculations performed by solving Eqs. (23) and (24), respectively, with Drude-like electric and magnetic responses and parameters listed in Table I. As the studied material has dispersive electric and magnetic responses, the results for the $\nu = \nu(\vec{\mathbf{k}})$ dispersion are much richer, as detailed in Figs. 5(c), 5(d), 6(c), and 6(d), which display the calculated results in the neighborhood of the electric and magnetic plasmon frequencies (see Table I).
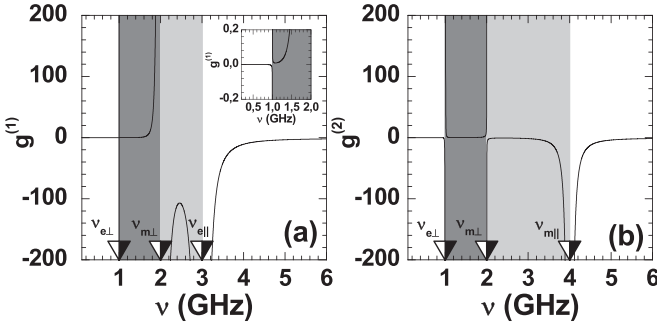
FIG. 4. Determinants (a) $g^{(1)}$ and (b) $g^{(2)}$ of the metric tensor $(g^{(1)}_{\mu\nu})$ and $(g^{(2)}_{\mu\nu})$, respectively, as functions of the frequency. Parameters for evaluating the Drude-like electric permittivity and magnetic permeability are given in Table I. White and gray areas in all panels correspond to the normal Minkowski metric $(-,+,+,+)$ and three-time metric $(-,-,-,+)$, respectively. Dark-gray area in panel (a) [(b)] corresponds to the metric $(-,+,+,-)$ [$(-,-,-,-)$]. Triangles at the bottom axes are located at the transition (plasmon) frequencies between different metrics.

One may note from Figs. 5(a), 5(c), 6(a), and 6(c) that, if the wave vector $\vec{\mathbf{k}}$ is paralell to the z axis (the anysotropy axis of both $\overset{\leftrightarrow}{\epsilon}$ and $\overset{\leftrightarrow}{\mu}$), then one may obtain, due to the Drude-like dielectric and magnetic responses considered here, two different solutions from Eq. (23) which are also solutions
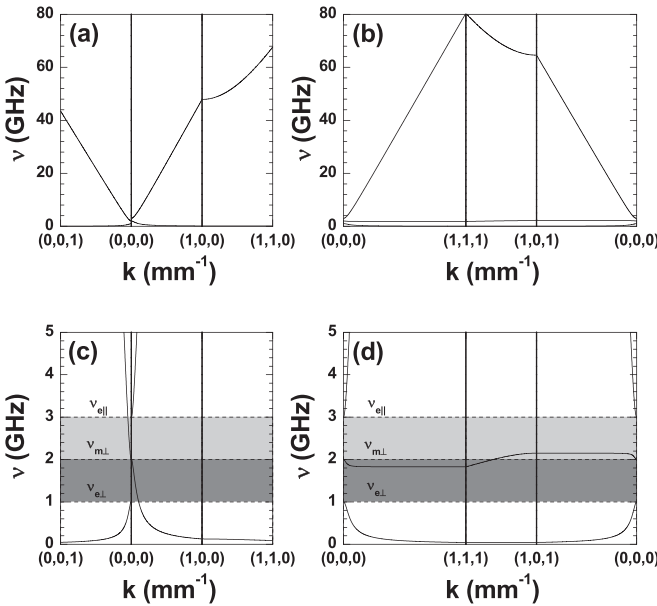

FIG. 5. Dispersion relation $\nu = \nu(\vec{\mathbf{k}})$ [$\nu = \omega/(2\pi)$] obtained from Eq. (23). Results were obtained by using the set of parameters displayed in Table I. Panels (c) and (d) show a zoom of the band structures depicted in panels (a) and (b), respectively, in the neighborhood of the electric and magnetic plasmon frequencies. White and gray areas correspond to the normal Minkowski metric $(-,+,+,+)$ and three-time metric $(-,-,-,+)$, respectively, whereas dark-gray area corresponds to the metric $(-,+,+,-)$. Horizontal dashed lines in panels (c) and (d) correspond to the plasmon-frequency values at which transitions between different metrics take place.
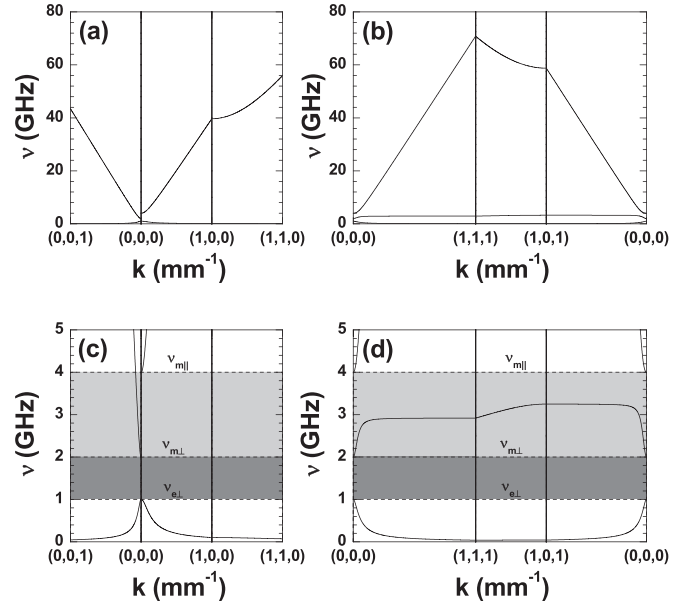

FIG. 6. As in Fig. 5, but for results obtained from Eq. (24). White and gray areas correspond to the normal Minkowski metric $(-,+,+,+)$ and three-time metric $(-,-,-,+)$, respectively, whereas dark-gray area corresponds to the metric $(-,-,-,-)$.

of Eq. (24). If the wave vector $\vec{\mathbf{k}}$ is neither perpendicular nor parallel to the z axis, then the nonseparability of the spatial components of $\vec{\mathbf{k}}$, together with the Drude-like dielectric and magnetic responses, lead to three different modes obtained from Eq. (23) and three other different solutions coming from Eq. (24) [cf. Figs. 5(b), 5(d), 6(b), and 6(d)]. As in the case of nonmagnetic materials discussed in the previous section, the frequency dependence of the components of $\overset{\leftrightarrow}{\epsilon}$ and $\overset{\leftrightarrow}{\mu}$ determines the number of subbands which may be obtained by solving Eqs. (23) and (24).

Let us now calculate the photonic density of states (DOS) which is connected with the band structure of the photonic crystal. The DOS is defined as the number of photonic states per unit of frequency and volume, i.e.,

$$\rho(\omega) = \frac{1}{\mathcal{V}} \sum_{\vec{\mathbf{k}}} \delta[\omega - \omega(\vec{\mathbf{k}})], \qquad (31)$$

where $\mathcal{V}$ is the system volume or, alternatively,

$$\rho(\omega) = \frac{1}{(2\pi)^3} \int_\Sigma \frac{1}{|\nabla_{\vec{\mathbf{k}}}[\omega - \omega(\vec{\mathbf{k}})]|} \, d\sigma, \qquad (32)$$

where Σ is the isofrequency surface obtained from the dispersion at a given value of the wave frequency. In Fig. 7 the DOS is depicted as a function of the incoming wave frequency. Figures 7(a) and 7(b) were obtained for the particular dispersion $\omega = \omega(\vec{\mathbf{k}})$ determined by the metric tensors $(g^{(1)}_{\mu\nu})$ and $(g^{(2)}_{\mu\nu})$, respectively. As expected, we find that the DOS diverges in the frequency regions corresponding to the hyperbolic metamaterial metrics $(-,-,-,+)$ and $(-,+,+,-)$, opening up the possibility of bulk propagating modes with unbound wave vectors in contrast with a vacuum [25].
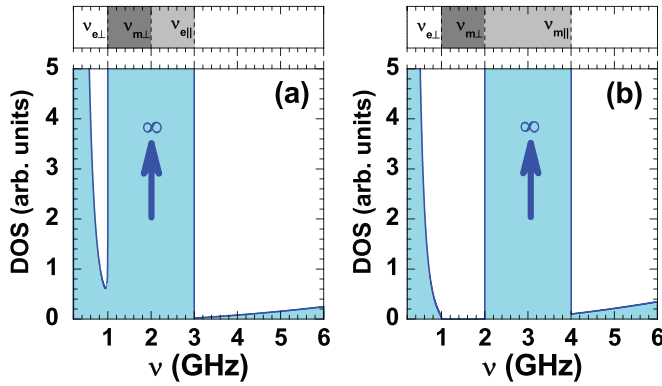
FIG. 7. (Color online) Photonic density of states as a function of the wave frequency, corresponding to metric tensors (a) $(g_{\mu\nu}^{(1)})$ and (b) $(g_{\mu\nu}^{(2)})$. Parameters for evaluating the Drude-like electric permittivity and magnetic permeability are given in Table I. White and gray areas at the top of both panels correspond to the normal Minkowski metric $(-,+,+,+)$ and three-time metric $(-,-,-,+)$, respectively. Dark-gray area at the top of panel (a) [(b)] corresponds to the metric $(-,+,+,-)$ $[(-,-,-,-)]$, whereas vertical dashed lines correspond to the plasmon frequencies at which transitions between different metrics take place.

For the Drude-like electric and magnetic responses considered in the present study, the DOS corresponding to the modes obtained from Eq. (23) does not vanish in the frequency axis. Therefore, there is no complete frequency gaps appearing in the corresponding band structure. In other words, it is possible to observe small frequency gaps for some particular directions of $\vec{k}$ (cf. solid lines in Fig. 5), but it is also possible to find other directions of the wave vector for which such gaps do not exist. In contrast, the DOS corresponding to the modes obtained from Eq. (24) vanishes in the region with metric $(-,-,-,-)$. As a consequence, a complete frequency gap is expected to occur in this frequency range, i.e., the frequency bandwidth with metric $(-,-,-,-)$ corresponds to a frequency gap for every possible direction of the wave vector.

IV. CONCLUSION

The metric signature topological transitions, with frequency-dependent and anisotropic dielectric and magnetic responses, are examined in the present work. The components

of the reciprocal-space metric tensor depend upon both the electric permittivity and magnetic permeability of the metamaterial, which are taken as Drude-like dispersive models. A thorough study is presented of the frequency dependence of the metric tensor which leads to the possibility of topological transitions of the isofrequency surface determining the wave dynamics inside the medium, to a diverging photonic density of states at some range of frequencies, and to the existence of large wave vectors modes propagating through the metamaterial.

In summary, metric signature topological transitions associated with the propagation of electromagnetic waves in a dispersive metamaterial have been theoretically analyzed assuming Drude-type electric and magnetic responses. As the photonic DOS is related to the volume enclosed by the corresponding isofrequency surface, we have found infinite DOS in the case of the hyperbolic isofrequency surface within the lossless effective medium limit. One might conjecture that the inclusion of loss should limit these infinite values of $\vec{k}$ to the more realistic case of very large but finite $\vec{k}$. This phase transition is characterized by the existence of eletromagnetic states with wave vectors extremely large compared to the allowed wave vectors in a vacuum, enhancing light-matter interactions and quantum related phenomena such as spontaneous emission. We conclude, therefore, that the dispersive nature of the metamaterial offers a myriad of possibilities to explore. By an appropriate change of the wave frequency it is possible to tune a specific reciprocal-space metric and study a wide variety of physical phenomena associated to the various isosurfaces. In the case of hyperbolic metamaterials $(-,-,-,+)$, for instance, exotic and remarkable properties such as no diffraction limit and large $\vec{k}$ propagating modes have been reported in the literature [26,27]. On the other hand, for the particular $(-,-,-,-)$ metric a complete band gap is found. In this way, we do hope the present study will contribute to further investigations on the realization of metamaterial-based new photonic devices.

[1] T. W. B. Kibble and G. R. Picket, Phil. Trans. R. Soc. **366**, 2793 (2008).

[2] E. Yablonovitch, Phys. Rev. Lett. **58**, 2059 (1987).

[3] S. John, Phys. Rev. Lett. **58**, 2486 (1987).

[4] U. Leonhardt and T. G. Philbin, New J. Phys. **8**, 247 (2006).

[5] I. I. Smolyaninov and E. E. Narimanov, Phys. Rev. Lett. **105**, 067402 (2010).

[6] H. N. S. Krishnamoorthy, Z. Jacob, E. Narimanov, I. Kretzschmar, and V. M. Menon, Science **336**, 205 (2012).

[7] I. I. Smolyaninov and Y. J. Hung, J. Opt. Soc. Am. B **28**, 1591 (2011).

[8] I. I. Smolyaninov, E. Hwang, and E. E. Narimanov, Phys. Rev. B **85**, 235122 (2012).

[9] I. I. Smolyaninov, Y.-J. Hung, and E. Hwang, Phys. Lett. A **376**, 2575 (2012).

[10] I. I. Smolyaninov, Phys. Rev. D **85**, 114013 (2012).

[11] A. J. Hoffman, L. Alekseyev, S. S. Howard, K. J. Franz, D. Wasserman, V. A. Podolskiy, E. E. Narimanov, D. L. Sivco, and C. Gmachl, Nat. Mater. **6**, 946 (2007).

[12] C. M. Soukoulis, S. Linden, and M. Wegener, Science **315**, 47 (2007).

[13] M. Wilson, Phys. Today **60**(2), 19 (2007).

[14] N. I. Zeludhev, Science **328**, 582 (2010).

[15] V. G. Veselago, Sov. Phys. Usp. **10**, 509 (1968); R. A. Shelby, D. R. Smith, and S. Schultz, Science **292**, 77 (2001); W. L. Barnes, A. Dereux, and T. W. Ebbesen, Nature (London) **424**, 824 (2003).

[16] S. A. Ramakrishna, Rep. Prog. Phys. **68**, 449 (2005); E. Ozbay, Science **311**, 189 (2006); J. B. Pendry, D. Schurig, and D. R. Smith, *ibid.* **312**, 1780 (2006).

[17] D. R. Smith, W. J. Padilla, D. C. Vier, S. C. Nemat-Nasser, and S. Schultz, Phys. Rev. Lett. **84**, 4184 (2000).

[18] J. Li, L. Zhou, C. T. Chan, and P. Sheng, Phys. Rev. Lett. **90**, 083901 (2003).

[19] H. Jiang, H. Chen, H. Li, Y. Zhang, and S. Zhu, Appl. Phys. Lett. **83**, 5386 (2003).

[20] M. Liscidini and L. C. Andreani, Phys. Rev. E **73**, 016613 (2006).

[21] S. B. Cavalcanti, M. de Dios-Leyva, E. Reyes-Gómez, and L. E. Oliveira, Phys. Rev. E **75**, 026607 (2007).

[22] S. Kocaman, R. Chatterjee, N. C. Panoiu, J. F. McMillan, M. B. Yu, R. M. Osgood, and D. L. Kwong, and C. W. Wong, Phys. Rev. Lett. **102**, 203905 (2009).

[23] J. Schilling, Nat. Photon. **5**, 449 (2011).

[24] E. Reyes-Gómez, D. Mogilevtsev, S. B. Cavalcanti, C. A. A. Carvalho, and L. E. Oliveira, Europhys. Lett. **88**, 24002 (2009); D. Mogilevtsev, F. A. Pinheiro, R. R. dos Santos, S. B. Cavalcanti, and L. E. Oliveira, Phys. Rev. B **82**, 081105(R) (2010); C. A. A. de Carvalho, S. B. Cavalcanti, E. Reyes-Gómez, and L. E. Oliveira, *ibid.* **83**, 081408(R) (2011).

[25] Z. Jacob, J.-Y. Kim, G. V. Naik, A. Boltasseva, E. E. Narimanov, and V. M. Shalaev, Appl. Phys. B **100**, 215 (2010).

[26] M. Noginov, M. Lapine, V. Podolskiy, and Y. Kivshar, Opt. Express **21**, 14895 (2013).

[27] I. I. Smolyaninov, B. Yost, E. Bates, and V. N. Smolyaninova, Opt. Express **21**, 14918 (2013).